

Do thermal effects always contribute to spin pumping signals?

Paul Noël¹, Maxen Cosset-Cheneau¹, Victor Haspot², Vincent Maurel³, Christian Lombard³, Manuel Bibes², Agnès Barthelémy², Laurent Vila¹, Jean-Philippe Attané¹

¹Univ. Grenoble Alpes, CNRS, CEA, Grenoble INP, IRIG-SPINTEC, F-38000 Grenoble, France

²Unité Mixte de Physique, CNRS, Thales, Université Paris-Sud, Université Paris-Saclay, Palaiseau, France

³Univ. Grenoble Alpes, CEA, CNRS, IRIG-SYMMES, F-38000 Grenoble, France

Spin pumping by ferromagnetic resonance is one of the most common technique to determine spin hall angles, Edelstein lengths or spin diffusion lengths of a large variety of materials. In recent years, rising concerns have appeared regarding the interpretation of these experiments, underlining that the signal could arise purely from thermoelectric effects, rather than from spin pumping and spin-charge interconversion. Here, we propose a method to evaluate the presence or absence of thermal effects in spin pumping signals, by combining bolometry and spin pumping by ferromagnetic resonance measurements, and comparing their timescale. Using a cavity to perform the experiments on Pt/NiFe and LSMO/Pt samples, we conclude on the absence of any measurable thermoelectric contribution such as the spin Seebeck and Anomalous Nernst effects.

Spinorbitronics is based on the interconversion of charge currents into spin currents, by the spin Hall Effect in bulk materials or by the Edelstein effect at surfaces and interfaces. Determining the spin to charge current conversion efficiency, *i.e.*, the spin Hall Angle or the inverse Edelstein length, and the spin diffusion length, is a key point to understand experimental results and develop applications. Materials with large spin Hall angles are indeed required for a variety of foreseen applications such as 3-terminal SOT MRAM [1], Magnetoelectric Spinorbit Logic [2] or Terahertz emitters [3]. Since the early 2000's several techniques have emerged to evaluate this conversion efficiency, using lateral spin valves [4], Spin Seebeck measurements [5], spin pumping FMR (SP-FMR) [6], magneto-optical Kerr effect measurements [7], etc. The Spin Pumping FMR technique has been widely used to evaluate the spin Hall angles and inverse Edelstein lengths of a large numbers of materials, including heavy metals [6,8,9], semiconductors [10], Rashba interfaces [11, 12] and topological insulators [13,14,15]. The reason of such a wide use relies on the compatibility of SP-FMR with any multilayer stack, and the absence of any complex and costly nanofabrication process, moreover ferromagnetic resonance was an already widely used spectroscopy technique to evaluate the dynamical and non-dynamical properties of ferromagnetic thin films

Even for a widely studied material as Platinum the estimated values of spin diffusion length and spin Hall angle determined by different techniques spread over more than one order of magnitude, with spin diffusion length ranging from 1.2 nm [16] to 11 nm [17] and spin Hall angle from 1.2% [18] to 38.7% [19]. This large discrepancy can be partially explained by differences in Pt resistivity [20] or accounted for by interface-related phenomena as spin memory-loss, but it still remains mostly unexplained [21]. In this particular context, concerns regarding the reliability of the SP-FMR technique have been pointed out. A thermal gradient could indeed arise at the ferromagnetic resonance, due to the energy absorption in the ferromagnetic layer [22,23,24]. Such a thermal gradient could give rise to several thermoelectric and spin-caloritronics contributions – in particular the Anomalous Nernst Effect (ANE) and the Spin Seebeck effect (SSE) – that would add up to the spin pumping Inverse Spin Hall Effect (ISHE) signal. In this picture, the signal would thus be due to a combination of the ISHE signal, the spin rectification effects (SRE) and thermal effects.

While the separation of ISHE from SRE has already been vastly discussed and can be achieved from the angular dependence in different measurement geometries [25,26,27], disentangling the ISHE signal from thermal effects remains an open question. While the Ordinary Seebeck Effect (OSE) and Ordinary Nernst Effect (ONE) contributions may be extracted from angular dependences, it is not the case of the ANE and SSE contributions, which possess an angular dependence similar to that of the ISHE signal. Recent analysis of spin-pumping results have even been based on the hypothesis that the observed signals are dominated by these thermal effects [23].

Figure 1 a) depicts the dynamical spin injection process as described by Tserkovnyak *et al.* [28], which is the model used to analyze the signal observed in spin pumping FMR measurements. As suggested by Yamanoi *et al.* [23], the additional dissipation at the FMR could lead to the appearance of a voltage along the x direction. The absorption at resonance would lead to a temperature increase of the ferromagnet, and thus to a thermal gradient perpendicular to the layers. This thermal gradient would lead to the injection of a pure spin current along Z towards the non-magnetic material, converted by ISHE into an electric field along X through a process known as the longitudinal Spin Seebeck effect as seen in figure 1.b. Owing to the existence of a thermal gradient, the Anomalous Nernst Effect in the FM layer could also appear, creating an electric field along X as depicted in figure 1c.

We propose to test these hypothesis in two multilayers. The first one is a Pt/NiFe bilayer, archetypal of spin pumping ISHE experiments [6, 8, 16, 18], with a large ANE coefficient in Py [29], and the second one is a LSMO/Pt bilayer, for which a high SSE contribution is expected [30].

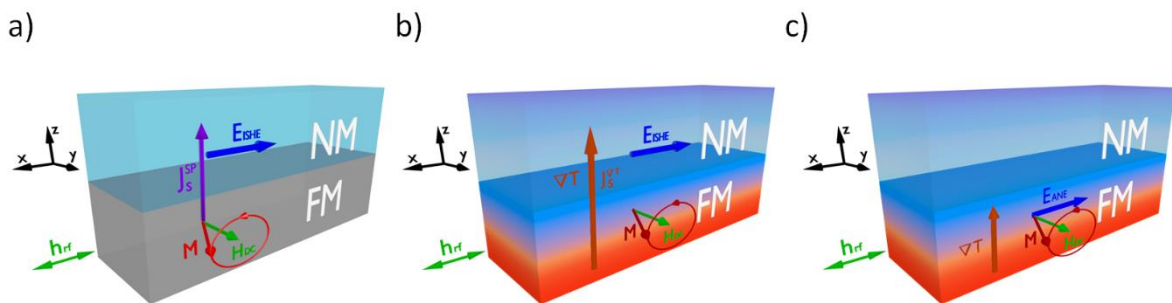


Figure 1: Schematic representation of the possible spin injection mechanisms at the FMR and of thermal gradient related effects. a) Dynamical spin injection. Because of the magnetization precession, the spin current J_S^{SP} is injected from the FM layer towards the NM layer. An electromotive force E_{ISHE} then arises along X, due to ISHE, which can be detected as a voltage in open circuit. b) Spin injection due to the thermal gradient. At the ferromagnetic resonance the temperature of the FM layer increases creating a thermal gradient ∇T along the z direction and thus a thermal spin current injection $J_S^{\nabla T}$. This spin current is then converted into an electromotive force E_{ISHE} . c) Thermal gradient within the ferromagnet could give rise to an Anomalous Nernst related electromotive force E_{ANE} .

The characteristic timescale of the FMR spin injection mechanism is the FMR precession period, which is of the order of the nanosecond. But the temperature increase timescale, the time needed to reach a thermal equilibrium, is of several seconds [31,32]: thermal and non-thermal effects have different dynamics. We thus propose a technique that can be adapted to any SP-FMR experiment to

disentangle the two mechanisms, by measuring the time dependence of the spin pumping signal and of the temperature increase.

We performed SP-FMR measurements on a $\text{SiO}_2/\text{Pt}(10)/\text{Py}(20)$ multilayer, on a $2.4 \times 0.4 \text{ mm}^2$ structure positioned in a Bruker MS5 loop gap cavity. The amplitude of the rf magnetic field h_{rf} was determined by measuring the Q factor with the sample placed inside the cavity [27]. We performed a FMR measurement at different sweeping rates, at a power of 100 mW. The scheme of the measurement is shown in figure 2 a), and consists in the measurement of the voltage at the ferromagnetic resonance. As seen in figure 2 b) and c) in both the parallel and antiparallel configurations, the signal is fully symmetric and independent of the sweeping time.

Regarding the possible contribution of Spin Rectifications Effects in Py, the out-of-plane angular dependence has also been performed (cf. figure 2 d). The obtained symmetric signal can be fitted with the ISHE angular dependence model described in reference [27] as $\sin(\Theta_M)$ with Θ_M being the magnetization angle respect to the out of plane direction.. This demonstrates that the contribution of spin rectification voltages are negligible. This also excludes any contribution of the Ordinary Seebeck effect, which would be field independent, and of the Nernst effect, which would depend on the applied field perpendicular to the thermal gradient. The signal is also linear with the power (cf. figure 2 e) indicating a negligible change of magnetization when increasing Power. The signal possesses the ISHE angular dependence, and there is no trace of thermal drift, which implies that if there is a thermal component to the signal, a steady state of thermal equilibrium has to be reached in a characteristic time well below one second.

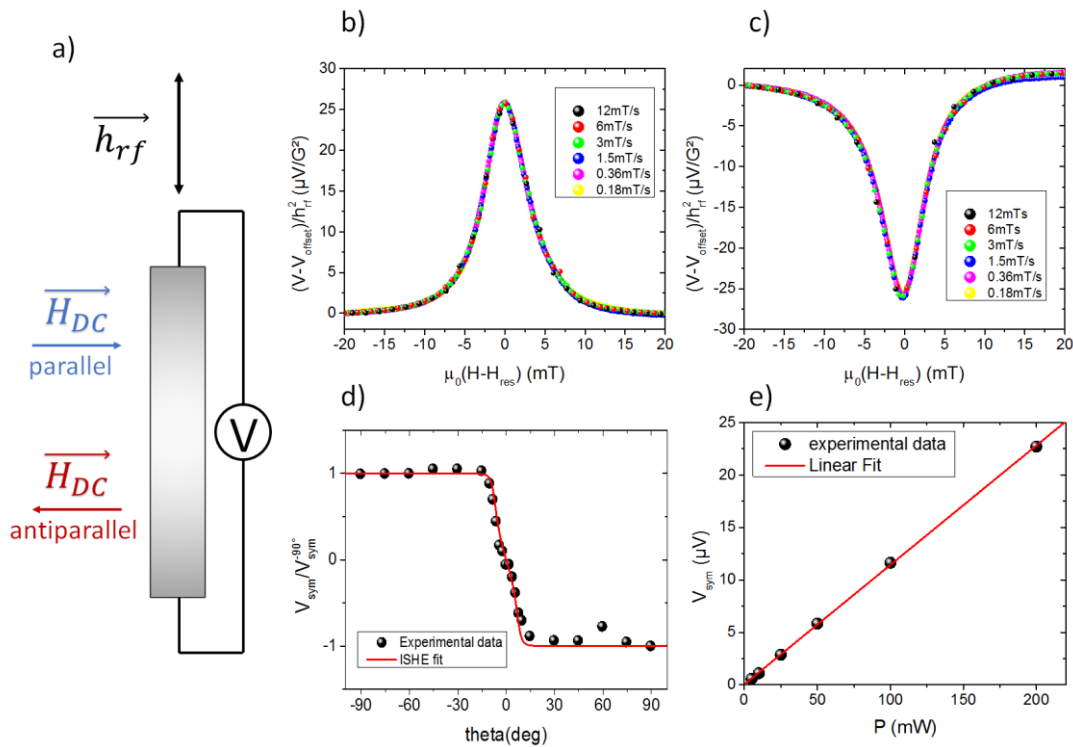


Figure 2: a) Schematic representation of the measurement device used to detect spin pumping ISHE at resonance in the $\text{Pt}(10)/\text{Py}(20)$ sample (top view). b) Signal obtained in the in-plane parallel configuration for various sweeping rates, normalized by the square of the rf magnetic field h_{rf}^2 for a power of 100mW c) Similar measurement in the in-plane antiparallel configuration d) Out-of-plane angular dependence of the spin signal fitted using the ISHE angular dependence provided in ref [27] e) Power dependence of the symmetric part of the signal as a function of the microwave power in the parallel configuration.

Let us now evaluate this characteristic time. A temperature increase can occur at the ferromagnetic resonance, due to the increased microwave absorption at resonance [22,31,32,33]. To evaluate the time dependence of this effect, we adopt the measurement scheme shown in figure 3 a), where the field is applied out of plane to avoid ISHE or SRE voltage contribution. We used a fixed DC current of 1 mA, fixed power of 100 mW and measured the change of resistance at resonance, known as the bolometric effect. As can be seen on figure 3 b) we observe an increase of resistance at resonance; more importantly, this increase is highly dependent on the field sweeping rate. The resistance increases from 7.2 ± 1 m Ω for a sweeping rate of 12 mT/s, to 28.5 ± 1 m Ω for a sweeping rate of 0.18 mT/s. The result is in stark contrast with fig. 2 where the signal is independent on the sweeping rate. The temperature increase characteristic time is thus of several seconds, as the time spent near resonance at a sweeping rate of 0.18 mT/s is of 20 s for a linewidth of 3.5 mT. This timescale is similar to what has been observed in previous Electrically Detected FMR experiments [31, 32].

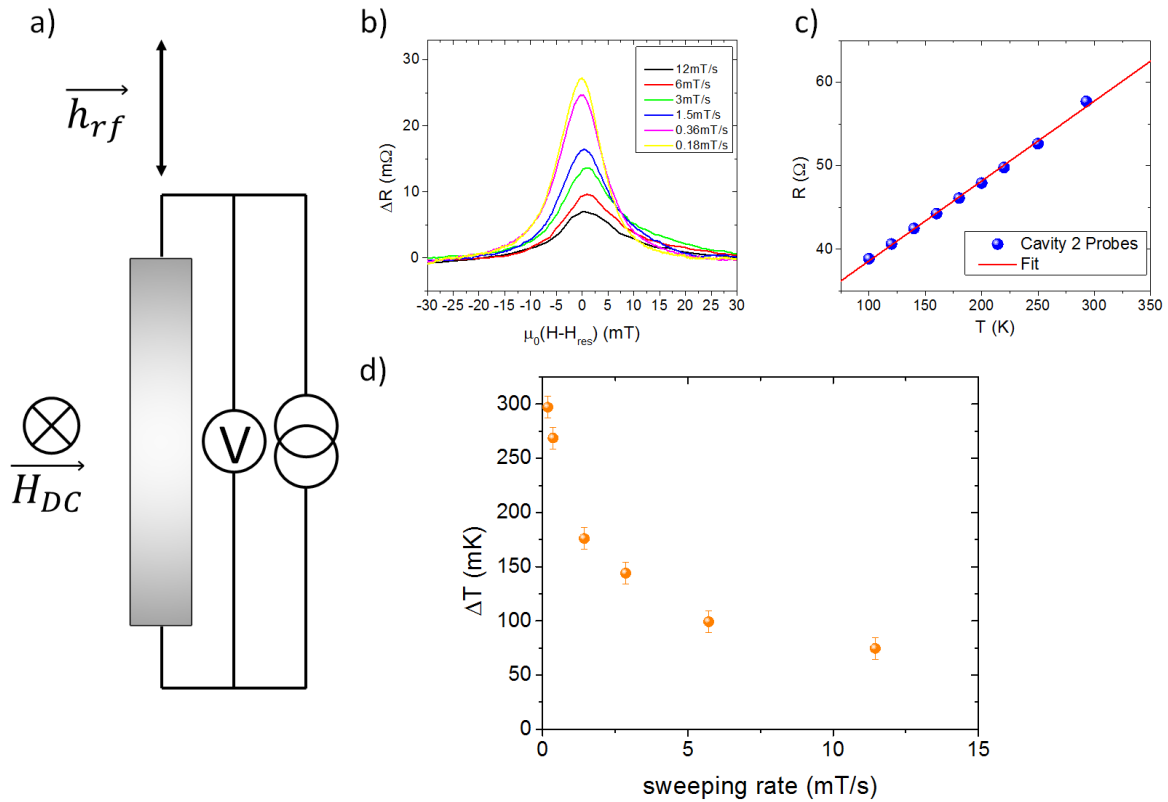


Figure 3: a) Schematic representation of the measurement device used to detect a resistance change at resonance in the Pt(10)\Py(20) sample (top view). b) Change of the two probes resistance around the resonance field, for various field sweeping rates (with base resistance subtracted). c) Resistance of the sample as a function of the temperature, measured in a 2 probes configuration on the same sample. The slope value is 96 ± 2 m Ω /K d) Temperature change as a function of the sweeping rate, estimated from the increase of resistance at resonance.

We estimate the corresponding temperature increase using the temperature dependence of the resistance of the sample measured inside the cavity (cf. figure 3c). The linear behavior of the resistance leads to a temperature dependence of 96 ± 2 m Ω /K in a range from 100K to Room temperature. The temperature increase as a function of the sweeping rate is shown in figure 3d. The

maximum temperature increase is small, of 297 ± 10 mK for the slowest sweeping rate, and only of 75 ± 10 mK for the fastest. The temperature increase is thus found to be strongly dependent on the sweeping time, the thermal equilibrium is not reached after several seconds near resonance. Therefore, any effect originating from a thermal gradient should vary with the sweeping time. The spin signals measured in the configuration of fig. 2 being totally independent of the sweeping time, we can conclude that in $\text{SiO}_2 \backslash \backslash \text{Pt}(10) \backslash \backslash \text{Py}(20)$ the Longitudinal Spin Seebeck Effect and anomalous Nernst effects are negligible, and that the observed signals are due to spin pumping and inverse spin Hall effect.

In order to verify this lack of thermal contribution we also performed a combined bolometric and SP-FMR measurements on a $\text{LSAT} \backslash \backslash \text{La}_{0.7}\text{Sr}_{0.3}\text{MnO}_3(13.8) \backslash \backslash \text{Pt}(8.2)$ sample, measured along the [100] direction. $\text{La}_{0.7}\text{Sr}_{0.3}\text{MnO}_3$ (LSMO) possesses a high resistivity compared to Permalloy and Platinum moreover the LSMO \backslash \backslash Pt structure is expected to possess a smaller ANE coefficient but a larger SSE contribution than Py \backslash \backslash Pt as demonstrated in Longitudinal Spin Seebeck experiments [30]. Therefore the possible contribution of SSE in this multilayer is expected to be enhanced compared to Pt \backslash \backslash Py. In figures 4b and 4c similarly to the case of Pt \backslash \backslash Py we can see that the thermal equilibrium is still not reached even for the slowest sweeping rate, the total temperature increase is of comparable amplitude and up to 199 ± 3 mK. As can be seen in figure 4e and 4f, the obtained spin signal is independent on the sweeping rate. Here again, this shows that in this system the ANE and SSE contributions are negligible compared to the spin pumping ISHE signal.

We would like to point out the fact that the NM and FM stacking order is inverted in the Pt \backslash \backslash Py sample. This leads to a spin signal of opposite sign when compared to LSMO \backslash \backslash Pt and previous results on Co \backslash \backslash Pt [9], as expected for ISHE symmetries [34]. The normalized ISHE signal is the ISHE voltage divided by the square of the rf field, the width and the total resistance of the device. The obtained values are of $0.78 \text{ mV} \cdot \text{G}^{-2} \cdot \Omega^{-1} \cdot \text{m}^{-1}$ in LSMO \backslash \backslash Pt and $1.11 \text{ mV} \cdot \text{G}^{-2} \cdot \Omega^{-1} \cdot \text{m}^{-1}$ in Pt \backslash \backslash Py, similar to the value of $0.85 \text{ mV} \cdot \text{G}^{-2} \cdot \Omega^{-1} \cdot \text{m}^{-1}$ to $1.13 \text{ mV} \cdot \text{G}^{-2} \cdot \Omega^{-1} \cdot \text{m}^{-1}$ that was previously reported in $\text{SiO}_2 \backslash \backslash \text{Co} \backslash \backslash \text{Pt}$ of similar thicknesses at X-band [9] indicating a similar injected spin currents in these three structures. A comparison with the signal obtained in ref [23] is not straightforward as the rf excitation field is not known, moreover the frequency used was of 2GHz instead of 9.7GHz in our case which would lead to differences in the precession cone angle and thus in the total signal [8].

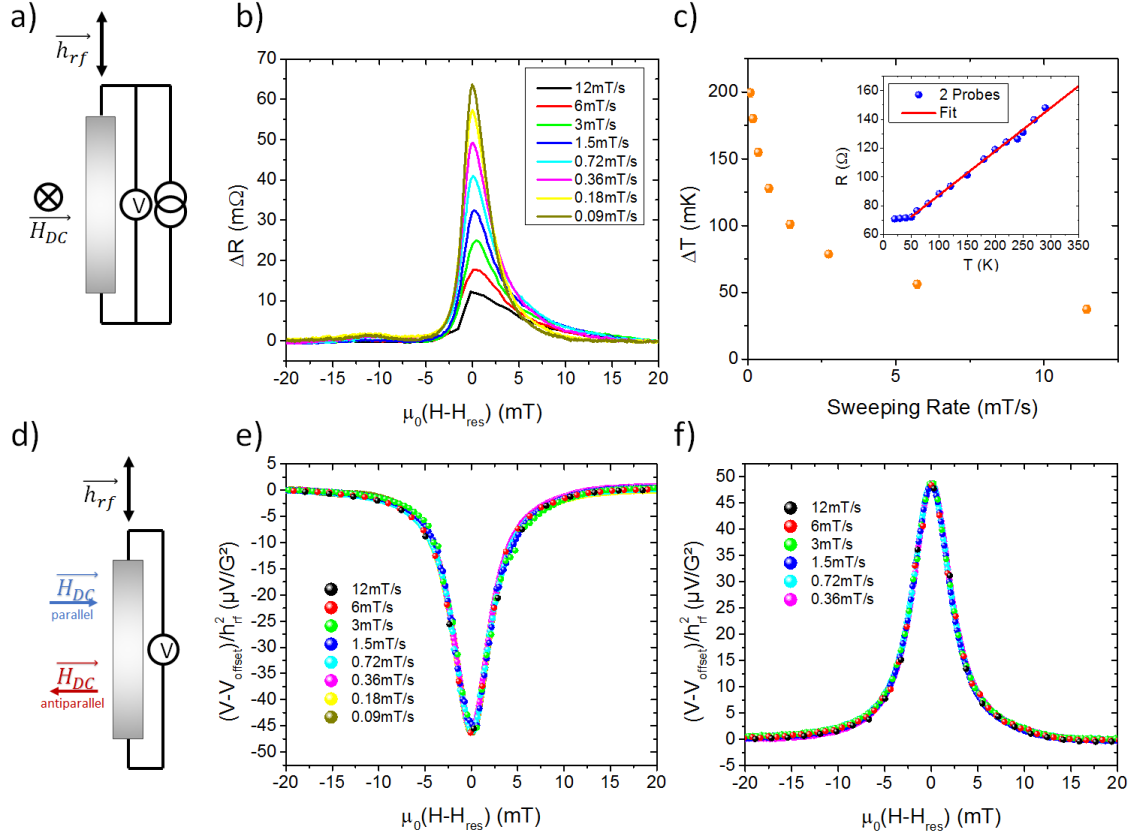


Figure 4: a) Schematic representation of the measurement device used to detect resistance change in the LSAT/La_{0.3}Sr_{0.7}MnO₃(13.8)/Pt(8.2) sample (top view). b) Change of resistance for various sweeping rate. c) Temperature change as a function of sweeping rate. Inset shows the resistance as a function of temperature, slope is of 303 ± 6 m Ω /K. d) Schematic representation of the measurement device used to detect spin pumping (top view). e) Signal obtained in the in-plane parallel configuration for various sweeping rates, normalized by the squared rf magnetic field h_{rf}^2 . f) Similar measurement in the in-plane antiparallel configuration

Another control experiment has been done to demonstrate the absence of thermal contribution to the spin pumping signal. The sample was placed in the parallel configuration and the external field was swept as fast as possible from 20 mT below the resonance to the resonance field H_{res} at a fixed rf power of 100mW. The sweeping rate in this experiments was limited to 1mT/s to avoid a large overshoot of the field when stopping at the resonance field and thus allowing a fast stabilization of the field comparable to our time resolution.

In a first step, a 5 mA current is applied in the sample, so that the signal variations correspond mostly to resistance variations. The voltage resulting due to Ohm's Law is of 5 μ V/m Ω using a current of 5mA while the total spin pumping signal is of around 10 μ V at a power of 100mW. The results, shown in figure 5 a), exhibits a resistance increase when reaching the resonance field. The time constant of the temperature increase is of around 10 seconds. In a second step, the same experiment is performed in the open circuit conditions commonly used for spin pumping experiments. In that case, the maximal signal is obtained immediately after reaching resonance field. This implies that the signal measured in open circuit conditions is not linked to the slow temperature increase at resonance but to the fast dynamical spin injection mechanism.

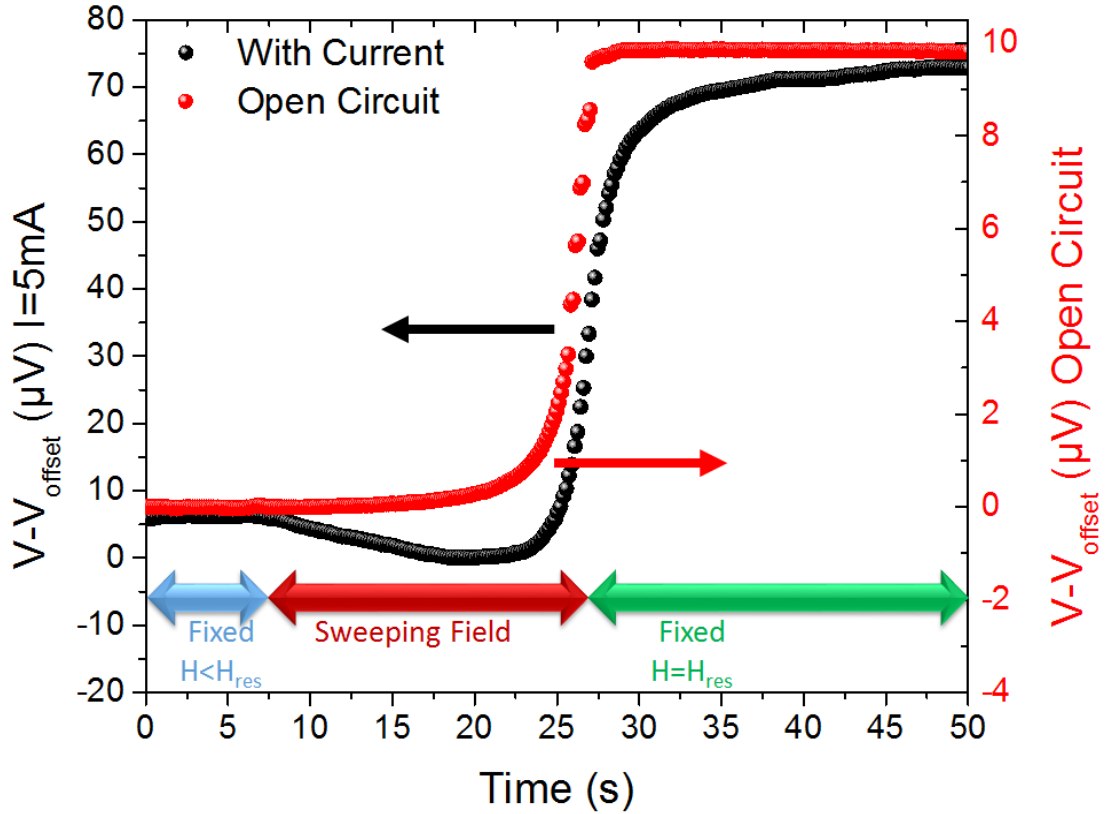


Figure 5: Change in the measured output voltage as a function of time during the sweeping of the field from out of resonance to resonance in the $\text{SiO}_2\backslash\text{Pt}(10)\backslash\text{Py}(20)$ sample for parallel to the plane configuration with an input current of 5mA (in black) and in open circuit conditions (in red).

To conclude, we observed in SP- FMR experiments in cavity that the temperature increase at resonance is limited to a few hundreds of mK, even at a large rf power of 100 mW, and is further reduced to dozens of mK for faster field sweeping around the resonance. Moreover, regarding the angular dependencies and the absence of link between the detected signal and the temperature increase at resonance, we can conclude that the SSE and ANE are absent in the signals for both $\text{SiO}_2\backslash\text{Pt}\backslash\text{Py}$ and $\text{LSAT}\backslash\text{LSMO}\backslash\text{Pt}$ multilayers, and that only dynamical spin injection is involved. The method presented here can be generalized to any multilayer and effect due to thermal gradients in spin pumping experiments. In particular, this method might be very interesting because of the growing interest in Rashba interfaces and topological insulators in spinorbitronics. Indeed, these two groups gather a large number of materials with very high thermoelectric figure of merit [35] such as Bi, Bi_2Se_3 , Bi_2Te_3 ... which could possibly give rise to non-negligible thermal signals, unrelated to spin-charge interconversion. It might also be useful to evaluate the contribution of the Unidirectional Spin Wave Propagation Induced Seebeck Effect in spin pumping experiments using thick YIG [36].

Acknowledgments:

We acknowledge the financial support by ANR French National Research Agency Toprise (ANR-16-CE24-0017), ANR French National Research Agency OISO (ANR-17-CE24-0026) and Laboratoire d'excellence LANEF (ANR-10-LABX-51-01). We are grateful to the EPR facilities available at the national TGE RPE facilities (IR 3443). We thank Jean-François Jacquot and Serge Gambarelli for their help and advices on the FMR measurement setup.

-
- ¹ Prenat, G., Jabeur, K., Di Pendina, G., Bouille, O., Gaudin, G., Spintronics-Based Computing. Springer International Publishing, 145–157 (2015)
- ² Maniapatruni, S., Nikonov, D.E., Lin, C.-C., Gosavi, T.A., Liu, H., Prasad, B., Huang, Y.-L., Bonturim, E., Ramesh, R., Young, I.A., *Nature* 565, 35 (2019)
- ³ Seifert, T., Jaiswal, S., Martens, U., Hannegan, J., Braun, L., Maldonado, P., Freimuth, F., Kronenberg, A., Henrizi, J., Radu, I., Beaurepaire, E., Mokrousov, Y., Oppeneer, P.M., Jourdan, M., Jakob, G., Turchinovich, D., Hayden, L.M., Wolf, M., Münzenberg, M., Kläui, M., Kampfrath, T., *Nature Photonics* 10, 483–488 (2016)
- ⁴ Vila, L., Kimura, T., Otani, Y.C., *Phys. Rev. Lett.* 99, 226604 (2007)
- ⁵ Uchida, K., Takahashi, S., Harii, K., Ieda, J., Koshibae, W., Ando, K., Maekawa, S., Saitoh, E., *Nature* 455, 778–781 (2008)
- ⁶ Saitoh, E., Ueda, M., Miyajima, H., Tatara, G., *Appl. Phys. Lett.* 88, 182509 (2006)
- ⁷ Kato, Y.K., Myers, R.C., Gossard, A.C., Awschalom, D.D., *Science* 306, 1910–1913 (2004)
- ⁸ Mosendz, O., Pearson, J.E., Fradin, F.Y., Bauer, G.E.W., Bader, S.D., Hoffmann, A., *Phys. Rev. Lett.* 104, 046601 (2010)
- ⁹ Rojas-Sanchez, J.C., Reyren, N., Laczkowski, P., Saverio, W., Attane, J.P., Deranlot, C., Jamet, M., George, J.M., Vila, L., Jaffres, H., *Phys. Rev. Lett.* 112, 106602 (2014)
- ¹⁰ Ando, K., Saitoh, E., *Nature Communications* 3, 629 (2012)
- ¹¹ Rojas-Sánchez, J.C., Vila, L., Desfonds, G., Gambarelli, S., Attané, J.P., De Teresa, J.M., Magén, C., Fert, A., *Nature Communications* 4, 2944. (2013)
- ¹² Sangiao, S., De Teresa, J.M., Morellon, L., Lucas, I., Martinez-Velarte, M.C., Viret, M., *Appl. Phys. Lett.* 106, 172403 (2015)
- ¹³ Jamali, M., Lee, J.S., Jeong, J.S., Mahfouzi, F., Lv, Y., Zhao, Z., Nikolić, B.K., Mkhoyan, K.A., Samarth, N., Wang, J.-P., *Nano Lett.* 15, 7126–7132 (2015)
- ¹⁴ Shiomi, Y., Nomura, K., Kajiwara, Y., Eto, K., Novak, M., Segawa, K., Ando, Y., Saitoh, E., *Phys. Rev. Lett.* 113, 196601 (2014)
- ¹⁵ Noel, P., Thomas, C., Fu, Y., Vila, L., Haas, B., Jouneau, P.H., Gambarelli, S., Meunier, T., Ballet, P., Attane, J.P., *Phys. Rev. Lett.* 120, 167201 (2018)
- ¹⁶ Zhang, W., Vlainck, V., Pearson, J.E., Divan, R., Bader, S.D., Hoffmann, A., *Appl. Phys. Lett.* 103, 242414 (2013)
- ¹⁷ Stamm, C., Murer, C., Berritta, M., Feng, J., Gabureac, M., Oppeneer, P.M., Gambardella, P., *Phys. Rev. Lett.* 119, 087203 (2017)
- ¹⁸ Feng, Z., Hu, J., Sun, L., You, B., Wu, D., Du, J., Zhang, W., Hu, A., Yang, Y., Tang, D.M., Zhang, B.S., Ding, H.F., *Phys. Rev. B* 85, 214423 (2012)
- ¹⁹ Berger, A.J., Edwards, E.R.J., Nembach, H.T., Karis, O., Weiler, M., Silva, T.J., *Phys. Rev. B* 98, 024402 (2018)
- ²⁰ Sagasta, E., Omori, Y., Isasa, M., Gradhand, M., Hueso, L.E., Niimi, Y., Otani, Y.C., Casanova, F., *Phys. Rev. B* 94, 060412 (2016)
- ²¹ Wesselink, R.J.H., Gupta, K., Yuan, Z., Kelly, P.J., arXiv:1901.00703 [cond-mat] (2019)
- ²² Yamanoi, K., Yokotani, Y., Kimura, T., *Appl. Phys. Lett.* 107, 182410 (2015)
- ²³ Yamanoi, K., Yokotani, Y., Kimura, T., *Phys. Rev. Applied* 8, 054031 (2017)
- ²⁴ Lin, W., Chien, C.L., arXiv:1804.01392 [cond-mat] (2018).
- ²⁵ Harder, M., Gui, Y., Hu, C.-M., *Physics Reports*, 661, 1–59 (2016)
- ²⁶ Azevedo, A., Vilela-Leao, L.H., Rodriguez-Suarez, R.L., Lacerda Santos, A.F., Rezende, S.M., *Phys. Rev. B* 83, 144402 (2011)
- ²⁷ Rojas-Sanchez, J.-C., Cubukcu, M., Jain, A., Vergnaud, C., Portemont, C., Ducruet, C., Barski, A., Marty, A., Vila, L., Attane, J.-P., Augendre, E., Desfonds, G., Gambarelli, S., Jaffrès, H., George, J.-M., Jamet, M., *Phys. Rev. B* 88, 064403 (2013)
- ²⁸ Tserkovnyak, Y., Brataas, A., Bauer, G.E.W., *Phys. Rev. B* 66, 224403 (2002)
- ²⁹ Holanda, J., Alves Santos, O., Cunha, R.O., Mendes, J.B.S., Rodríguez-Suárez, R.L., Azevedo, A., Rezende, S.M., *Phys. Rev. B* 95, 214421 (2017)
- ³⁰ Wu, B.W., Luo, G.Y., Lin, J.G., Huang, S.Y., *Phys. Rev. B* 96, 060402 (2017)
- ³¹ Goennenwein, S.T.B., Schink, S.W., Brandlmaier, A., Boger, A., Opel, M., Gross, R., Keizer, R.S., Klapwijk, T.M., Gupta, A., Huebl, H., Bihler, C., Brandt, M.S., *Appl. Phys. Lett.* 90, 162507 (2007)
- ³² Gui, Y.S., Mecking, N., Wirthmann, A., Bai, L.H., Hu, C.-M., *Appl. Phys. Lett.* 91, 082503 (2007)
- ³³ Hahn, C., de Loubens, G., Klein, O., Viret, M., Naletov, V.V., Ben Youssef, J., *Phys. Rev. B* 87, 174417 (2013)

³⁴ Schreier, M., Bauer, G.E.W., Vasyuchka, V.I., Flipse, J., Uchida, K., Lotze, J., Lauer, V., Chumak, A.V., Serga, A.A., Daimon, S., Kikkawa, T., Saitoh, E., Wees, B.J. van, Hillebrands, B., Gross, R., Goennenwein, S.T.B., J. Phys. D: Appl. Phys. 48, 025001 (2014)

³⁵ Goldsmid, H.J., Materials (Basel) 7, 2577–2592 (2014)

³⁶ Wang, P., Zhou, L. F., Jiang, S.W., Luan, Z.Z., Shu, D.J., Ding, H.F., Wu, D., Phys. Rev. Lett. 120, 047201 (2018)